ADVANCED HEALTHCARE MATERIALS
www.advhealthmat.de

Uplifting Antitumor Immunotherapy with Lymph-Node-Targeted and Ratio-Controlled Codelivery of Tumor Cell Lysate and Adjuvant

Guanhong Cui, Yinping Sun, Liping Qu, Cui Shen, Yu Sun, Fenghua Meng, Yiran Zheng, and Zhiyuan Zhong**

Cancer vaccines provide a potential strategy to cure patients. Their clinical utilization and efficacy is, however, limited by incomplete coverage of tumor neoantigens and unspecific and restricted activation of dendritic cells (DCs). Tumor cell lysates (TCLs) containing a broad spectrum of neoantigens, while are considered ideal in formulating personalized vaccines, induce generally poor antigen presentation and transient antitumor immune response. Here, intelligent polymersomal nanovaccines (PNVs) that quantitatively coload, efficiently codeliver, and responsively corelease TCL and CpG adjuvant to lymph node (LN) DCs are developed to boost antigen presentation and to induce specific and robust antitumor immunity. PNVs carrying CpG and ovalbumin (OVA) markedly enhance the maturation, antigen presentation, and downstream T cell activation ability of bone-marrow-derived dendritic cells and induce strong systemic immune response after tail base injection. Remarkably, PNVs carrying CpG and TCL cure 85% of B16-F10 melanoma-bearing mice and generate long-lasting anticancer immune memory at a low dose, protecting all cured mice from tumor rechallenge. These LN-directed PNVs being highly versatile and straightforward opens a new door for personalized cancer vaccines.

1. Introduction

Being one of the most cutting-edge and effective tumor therapies, cancer vaccines have elicited encouraging results and even potential cures in patients with melanoma and resected pancreatic cancer.[1] However, the efficacies and clinical applications of cancer vaccines are still hindered by limited coverage of tumor specific antigens (TSAs) and inadequate activation of dendritic cells (DCs).[2] Cancer vaccines typically stimulate DCs to process and present vaccine-loaded antigens (Ags) to activate T-cell-mediated killing of Ag-expressing cells.[2a] TSAs are neoantigens uniquely expressed by tumor cells and can generate tumor-specific immune responses without eliciting central or peripheral tolerance.[3] Tumor cell lysates (TCLs) are derived from whole tumor cells and contain abundant and diverse TSAs, thus allowing induction of a broad and durable antitumor immunity to minimize cancer immune escape.[4] In addition, as TCLs are generated from patient-specific tumor biopsies, TCL-based vaccines can combat tumor antigenic heterogeneity between patients, making TCL ideal candidates for formulating personalized vaccines.[2a] Nevertheless, direct administration of TCL with adjuvant yielded disappointing results in past clinical attempts.[5] The main contributing reasons include difficulties in delivering TCL to the cytosol of DCs in lymph nodes (LNs) and the propensity to trigger immune tolerance.[6]

To enhance LN-targeted delivery of Ags, multiple novel carrier systems have been reported.[7] However, these carriers are either tailored to load defined Ags or require modification of Ags, rendering them unsuitable for loading TCLs that contain diverse biomolecules with undefined nature. Delivery systems also need to be stable in circulation to minimize leakage of Ags, uptake efficiently by LN DCs, and rapidly release loaded cargos once in DC cytosol for efficient antigen presentation.[3a,6b]

Quantitative codelivering TCL and adjuvant to the same DC is key to optimal DC priming and generation of robust antitumor immunity without triggering tolerance.[2b,4d,8] Prolonged exposure to Ags in the absence of adjuvant usually triggers undesirable immune tolerance rather than immune activation.[9] Imperfect ratio of TCL to adjuvant might also promote tolerance due to the presence of healthy cell components in TCL while excessive adjuvants might lead to autoimmune diseases.[6a,10] Therefore,

G. Cui, Y. Sun, L. Qu, Y. Sun, F. Meng, Z. Zhong
Biomedical Polymers Laboratory
College of Chemistry
Chemical Engineering and Materials Science, and State Key Laboratory of Radiation Medicine and Protection
Soochow University
Suzhou 215123, P. R. China
E-mail: zyzhong@suda.edu.cn

C. Shen, Y. Zheng, Z. Zhong
College of Pharmaceutical Sciences
Soochow University
Suzhou 215123, P. R. China
E-mail: yrzheng@suda.edu.cn

The ORCID identification number(s) for the author(s) of this article can be found under https://doi.org/10.1002/adhm.202303690

DOI: 10.1002/adhm.202303690

precise control of the ratio between delivered TCL and adjuvant is essential to the efficacies of TCL-based vaccines.

Despite the advances in the field, the existing nanovaccines still suffer from inefficient coloading of TCL/adjuvant, poor ratio-controlled codelivery of cargo to LN DCs, and/or lack of responsive-release mechanism in DC cytosol.[4b,8,11]

Here, we developed intelligent polymersomal nanovaccines (PNVs) to quantitatively coload, LN-targeted codeliver, and efficiently corelease TCL and adjuvant CpG for eliciting specific and robust antitumor immune responses. TCL (or ovalbumin, OVA) and CpG could be coloaded in PNVs with near 100% efficiency for both, thus allowing quantitative control over the respective vaccine content by adjusting the added amount. The formed PNVs could specifically target to LNs, promote uptake of vaccine by LN DCs, and rapidly release cargo in the reducing environment of DC cytosol. PNVs coloading TCL and CpG (CpG/TCL@PNV) significantly enhanced DC maturation, induced tumor-specific and systemic immune responses, and substantially improved treatment outcome for solid and metastatic tumor. More importantly, PNVs promoted the generation of long-term immune memory for preventing tumor recurrence. Furthermore, PNVs could also load predefined Ag to serve as both therapeutic and prophylactic vaccines, demonstrating the broad applications of PNVs.

2. Results

2.1. Preparation and In Vitro Characterization of PNVs

PNVs were readily fabricated by adding a solution of poly(ethylene glycol)-*b*-poly(trimethylene carbonate-*co*-dithiolane trimethylene carbonate)–spermine (abbreviated as PEG–P(TMC-DTC)–SP) in *N*,*N*-dimethylformamide (DMF) into aqueous solution containing Ags and adjuvant CpG followed by dialysis (**Figure 1A**). PEG is longer than spermine so that PEG would preferentially present at the outer surface while spermine in the watery core. P(TMC-DTC) is a biodegradable polycarbonate containing pendant dithiolane groups that enable automatic cross-linking of vesicular membrane during fabrication and de-cross-linking in reducing conditions such as in the cytosol. When designed polymer mixed with CpG and TCL at 10 wt% of polymer, the formed PNVs could coload 100% CpG and 98% TCL added (Table S1, Supporting Information). Even when the total amount of TCL and CpG went up to 20 wt% of polymer, a high drug loading efficiency (DLE) at 91% could still be achieved for both TCL and adjuvant. In addition, the DLE for model protein OVA and CpG was also higher than 94%, demonstrating the feasibility of using PNVs to coload diverse Ags and adjuvant efficiently (Table S1, Supplementary Information). Furthermore, the loaded Ags and adjuvant could easily account for more than 18 wt% of carriers. With similar loading content, PNVs exhibited much enhanced coloading efficiency for TCL and CpG than nanovaccines formed by poly(lactic-co-glycolic acid) (PLGA) polymer or hybrid materials.[4b,11a,b]

PNVs coloading adjuvant CpG and TCL were ≈55 nm in size by dynamic light scattering (DLS) with an overall surface charge of ≈6.6 mV and exhibited vesicular structure under transmission electron microscope (TEM) (Figure 1B). PNVs coloading CpG and OVA (CpG/OVA@PNV) were stable without substantial size change in 10% fetal bovine serum (FBS) within 24 h, but dissociated rapidly in 10 mM glutathione (GSH) (Figure 1C). In the presence of 10 mM GSH, ≈80% loaded OVA was released within 10 h, while only 14% OVA was released in the absence of GSH (Figure 1D). These data collectively indicated that PNVs exhibited excellent stability but could rapidly release cargo once in cytoplasm.

2.2. PNVs Effectively Stimulate Bone-Marrow-Derived Dendritic Cells (BMDCs) In Vitro

Next, we evaluated the immunostimulatory impacts of PNVs on BMDCs. For in vitro experiments, PNVs loading 50 μg CpG (per mg PNVs), 49.2 μg OVA (per mg PNVs), or both (50 μg CpG + 49.2 μg OVA per mg PNVs with ratio at 1:0.98) were used. PNVs encapsulating CpG (CpG^{Cy5}@PNV) or OVA^{FITC} (OVA^{FITC}@PNV) effectively promoted the endocytosis of CpG or OVA (Figure 1E and Figure S1 (Supporting Information)) by BMDCs. Compared to the mixture of CpG, OVA, and empty PNVs (CpG + OVA + PNV), CpG/OVA@PNV significantly elevated the expression of maturation marker cluster of differentiation 86 (CD86) on BMDC (Figure 1F). CpG/OVA@PNV also promoted BMDCs' secretion of proinflammatory cytokines such as interleukin-12 (IL-12p70) and IL-6 by 22-fold and 1.3-fold, in comparison to the physical mixture group (Figure 1G,H). These data demonstrated that loading Ag and CpG in PNVs could substantially enhance BMDC activation and maturation. Furthermore, CpG/OVA@PNV also promoted Ag presentation by BMDCs and proliferation of SIINFEKL-specific OT-1 $CD8^+$ T cells most efficiently (Figure 1I,J). Interestingly, CpG/OVA@PNV induced higher CD86 expression, IL-12p70/IL-6 secretion, and antigen presentation of BMDCs than CpG@PNV (Figure 1F–H), implying that codelivery of Ag and adjuvant could stimulate BMDCs more effectively than delivering adjuvant only. We next evaluated the toxicity of CpG/OVA@PNV in vitro using 293T and L929 cells as models.[12] The results showed negligible toxicity even at 100 μg mL^{-1} (Figure S2, Supporting Information). Overall, PNVs coloading Ag and adjuvant could substantially enhance the Ag presentation abilities of BMDCs, thus promoting the downstream T cell activation with good safety.

2.3. PNVs Elicit Robust Immune Responses in Mice

PNVs specifically delivered Ag and CpG to draining LNs following tail base injection. Compared to free CpG, PNVs elicited a 20-fold increase in the amount of CpG in inguinal LNs (**Figure 2A,B**). More importantly, the fluorescent signal of CpG in inguinal LNs (iLNs) accounted for strikingly 50% of total signals in major organs, indicating that half of the injected dose accumulated in LNs (Figure 2A,C). The amount of signal in iLNs was even 2.7-fold higher than that in liver. PNVs exhibited significantly higher LN-targeting ability than most nanovaccines in the literature and comparable to the best existing LN-directed carriers to our knowledge,[13] substantially improving the bioavailability of Ag and adjuvant. The PNV-induced accumulation of Ag

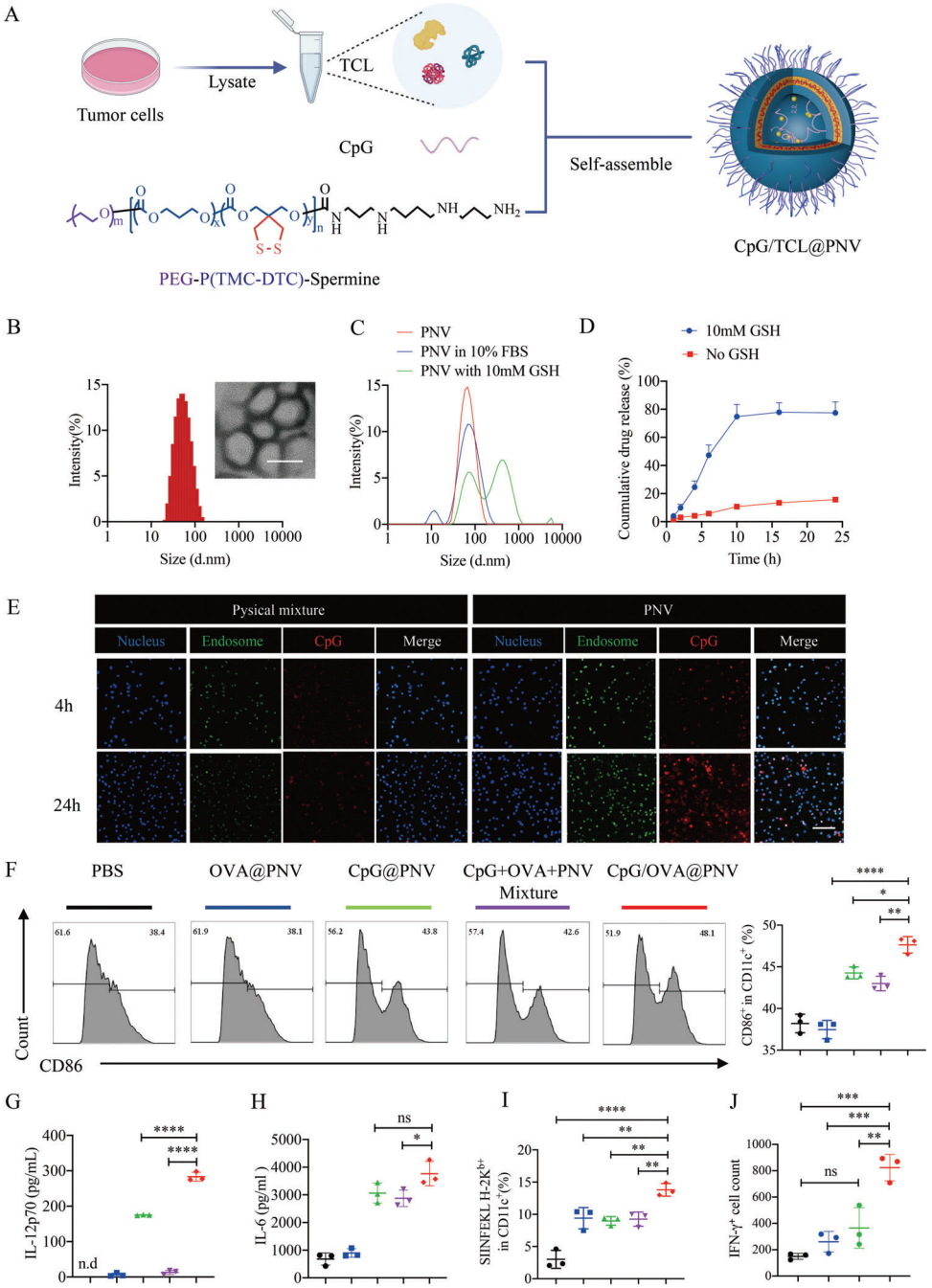

Figure 1. Preparation, characterization, and in vitro immune-stimulatory effects of PNVs. A) Scheme illustrating the preparation procedure of CpG/TCL@PNV. B) Size distribution of PNVs determined by DLS and TEM. Scale bar, 50 nm. C) Size change of PNVs in solution containing FBS or GSH. D) In vitro drug release kinetics of PNVs at 37 °C with or without 10 mM GSH ($n = 3$). E) Endocytosis of CpG^{Cy5}-loaded PNVs or free CpG^{Cy5} in BMDCs after coincubation for 4 and 24 h. Scale bar, 100 μm. F) Sample histogram and quantification of CD86 expression on BMDCs. G) Amount of BMDC-secreted proinflammatory cytokine IL-12p70 and H) IL-6 in culture medium determined by ELISA. I) SIINFEKL H-2 k^b expression on BMDCs after their coincubation with PNVs. J) PNV-treated BMDCs were coincubated with OT-1 $CD8^+$ T cells ($n = 3$). The number of IFN-γ^+ T cells from each group was evaluated via flow cytometer.

and CpG in LNs substantially enhanced the maturation of DCs in LN, allowing the percentage of $CD80^+CD86^+$ DCs to be 2.5-fold higher than that from the physical mixture group (Figure 2D,E).

PNVs also induced the generation of Ag-specific T cells in spleens. By using a common setup in literature,[14] we inoculated mice with tumor cells and then immunized mice with CpG/OVA@PNV or CpG/TCL@PNV (TCL generated from B16-F10 cells). Splenocytes were harvested 7 days after the last dose of immunization and pulsed with Ag OVA or TCL, respectively (Figure 2F). Enzyme linked immunospot (ELISpot)

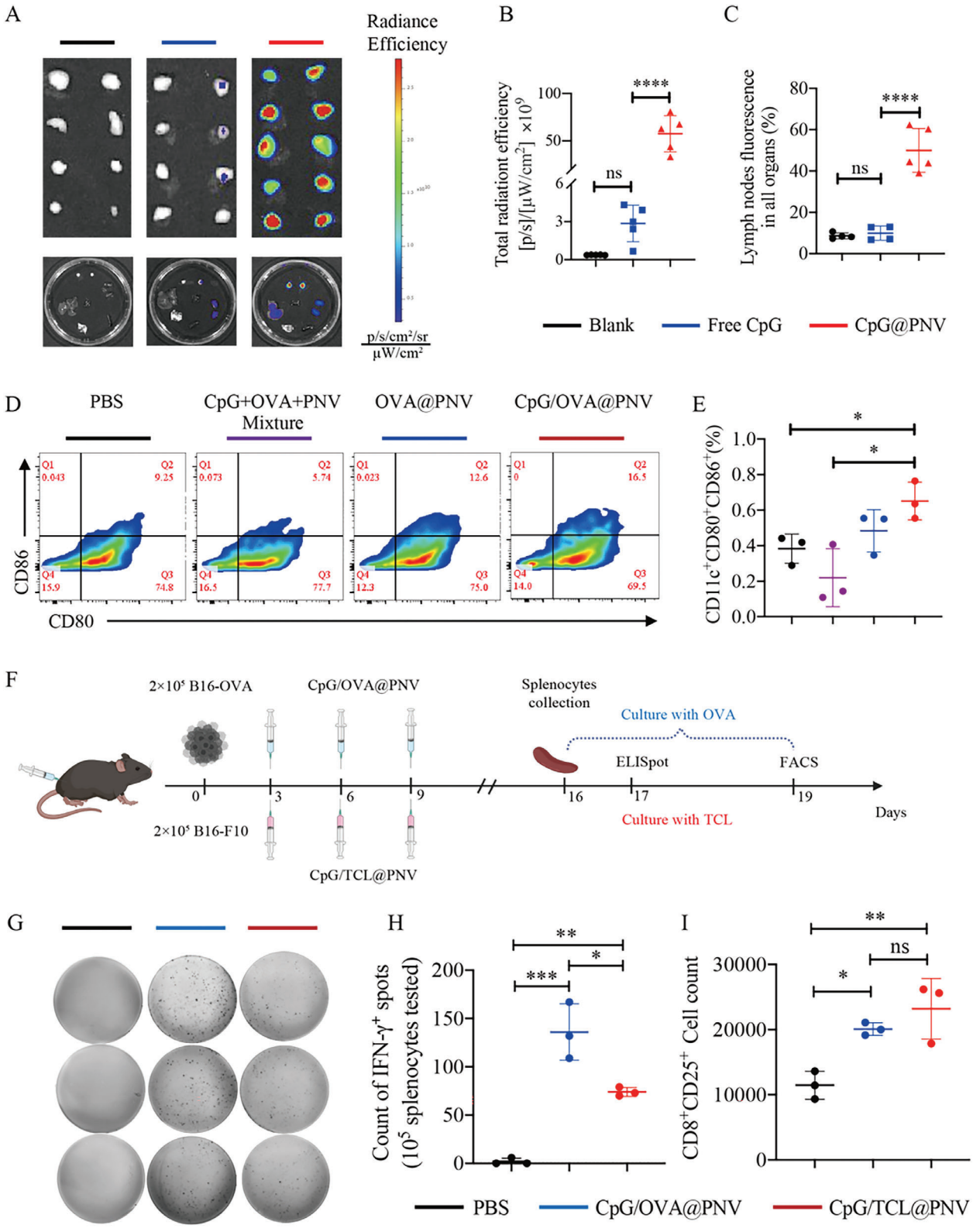

Figure 2. PNVs target to LNs and elicit tumor-specific immune responses in vivo. Accumulation of Cy7-labeled CpG (CpG^{Cy7}) in LNs and other organs after tail base injection of PBS, free CpG^{Cy7}, and PNVs loading CpG ^{Cy7} (20 μg CpG per mouse). A) IVIS images of inguinal LNs and B) quantification of LN fluorescence ($n = 4$–5). C) Percentage of LN fluorescence in signals from all organs. D) Expression of CD80 and CD86 by DCs in draining LNs at 24 h after injection ($n = 3$). E) Quantitative analysis of percentage of $CD11c^+CD80^+CD86^+$ cells in all lymph node cells. F) Timeline to analyze Ag-specific and activated T cells in spleen after immunization. G) Image and H) quantification of Ag-specific IFN-γ^+ T cells among splenocytes via ELISpot assay. I) Quantification of activated T cells by FACS ($n = 3$).

assay revealed that substantial number of interferon-γ (IFN-γ) producing T cells were present in both CpG/OVA@PNV and CpG/TCL@PNV groups, while negligible T cells recognizing OVA or TCL were observed in phosphate-buffered saline (PBS) group (Figure 2G,H). The number of activated $CD25^+CD8^+$ T cells from the nanovaccine groups was also significantly higher than that from PBS group (Figure 2I). Therefore, PNVs using either OVA or TCL as Ags could elicit Ag-specific T cells in vivo.

2.4. PNVs Effectively Eradicate Solid Tumors

To explore the optimal formulation for PNVs, we prepared PNVs loading with varying amounts of B16-F10 TCL, CpG, or their combination and conducted pilot therapy experiment in mice bearing subcutaneous melanoma (**Figure 3**A). For example, CpG/TCL@PNV (10/5) indicated that CpG/TCL was coencapsulated at 2:1 ratio and total 10 μg CpG together with 5 μg TCL was injected per mouse. In comparison to PBS group, TCL@PNV (5), the nanovaccine loading only TCL, yielded minimal antitumor effect, while CpG@PNV (10), the nanovaccine loading just adjuvant, suppressed 67% of tumor growth by day 22 after tumor inoculation (Figure 3B,C). The combination of CpG@PNV (10) and TCL@PNV (5) did not elicit significant efficacy improvement from that induced by CpG@PNV (10) alone. Notably, codelivering CpG and TCL in the same carrier via CpG/TCL@PNV (10/5) demonstrated enhanced tumor suppression efficacy with average tumor size only 25% and 76% of that from PBS group and CpG@PNV (10) group, respectively (Figure 3B,C). In the meantime, physical mixture of empty PNV, free CpG (10), and free TCL (5) elicited a much weaker therapeutic outcome than CpG/TCL@PNV (10/5). Therefore, TCL and CpG need to be coloaded and codelivered in PNVs to maximize antitumor efficacies.

CpG/TCL@PNVs with various CpG/TCL coloading dosages and ratios (5/5, 10/20, and 20/20) were then prepared with fixed PNV amount and compared their efficacy with that from CpG/TCL@PNV (10/5). CpG/TCL@PNV (5/5), with lower CpG amount than CpG/TCL@PNV (10/5), elicited weaker tumor inhibition as expected. Surprisingly, despite having higher Ag amount than CpG/TCL@PNV (10/5), CpG/TCL@PNV (10/20), lost efficacy completely and did not demonstrate any observable benefits over PBS. However, CpG/TCL@PNV (20/20), with both CpG and TCL amount increased to 20 μg, inducing the strongest efficacy with tumor size being 4% and 16% of that from PBS and CpG/TCL@PNV (10/5) groups, respectively (Figure 3B,C). Therefore, CpG/TCL@PNV (20/20) was employed in subsequent animal studies.

Then, we evaluated the long-term treatment outcome and survival rate of PNVs loading only Ag, only CpG, or Ag together with CpG (Figure 3D). CpG@PNV elicited complete response (CR) in 43% of mice, a much stronger efficacy than 14% from TCL@PNV (Figure 3E–G). Codelivering group CpG/TCL@PNV demonstrated superior efficacy over CpG@PNV by curing ≈86% of mice, substantially prolonging the survival rate of mice (Figure 3E–G). Thus, codelivering CpG and TCL by PNVs was crucial to achieve optimal treatment outcome.

2.5. PNVs Elicit $CD8^+$ T-Cell-Mediated Antitumor Efficacy and Long-Term Immune Memory

The depletion of $CD8^+$ T cell via infusing anti-CD8 antibody caused the complete loss of antitumor efficacy of CpG/TCL@PNV (**Figure 4**A–C), indicating that PNVs exert efficacy through $CD8^+$ T cells.

Generation of long-term antitumor immune memory is vital for preventing tumor recurrence. We also tested the efficacy of PNVs in minimizing tumor relapse in murine subcutaneous melanoma model (Figure 4D). CpG/TCL@PNV-cured mice (from therapy experiment in Figure 3D–F) and equal number of healthy mice were rechallenged with B16-F10 tumor cells on 53 days after last PNV treatment. Strikingly, CpG/TCL@PNV pretreatment protected all mice from tumor outgrowth, indicating that CpG/TCL@PNV could 100% prevent melanoma recurrence (Figure 4E).

Subsequently, we evaluated the memory T cells in PNV-cured mice 120 days post initial tumor cell inoculation (93 days after last PNV treatment) (Figure 4D). Compared to nonimmunized mice, the number of $CD3^+$ T cells and $CD8^+$ T cells in spleens was increased more than twofold in cured mice (Figure 4F). Moreover, $CD4^+$ central memory T cells ($CD44^+CD62L^+$) and $CD4^+$ effector memory T cells ($CD44^+CD62L^-$) in spleens were substantially enhanced by 17-fold and 14-fold, respectively (Figure 4F). $CD4^+$ effector memory T cells and $CD8^+$ central memory T cells in peripheral blood mononuclear cells (PBMCs) were also significantly elevated in CpG/TCL@PNV-cured mice (Figure 4G). Thus, our study indicated that CpG/TCL@PNV could induce long-term immune memory to prevent tumor recurrence.

2.6. PNVs Suppress Tumor Metastasis

Metastasis usually takes place in later stage of tumor development and accounts for most of the cancer deaths. The effectiveness of PNVs against metastasis was also tested. B16-F10 cells were intravenously injected to induce lung metastasis before vaccine treatment and then lungs from four mice in each group were harvested for observation on day 24 after tumor inoculation (**Figure 5**A). Nanovaccine loaded with only TCL or CpG (TCL@PNV or CpG@PNV), just partially protected mice from tumor metastasis (Figure 5B). On the contrary, CpG/TCL@PNV yielded potent antimetastasis efficacy. Lung morphology and hematoxylin and erosin (H&E) staining revealed that there were no observable metastases spots in lung tissues after four immunizations (Figure 5B). Compared with the lung weight of CpG/TCL@PNV group, the lung weight of PBS group increased approximately threefold, while the lung weight of TCL@PNV group increased approximately twofold due to excessive tumor metastasis (Figure 5C). Although no significant difference was detected in lung weight between CpG/TCL@PNV and CpG@PNV group, the median survival time of CpG/TCL@PNV was 10 days longer than that from CpG@PNV. 40% of mice in CpG/TCL@PNV remained alive even after tumor inoculation for 46 days, while mice in CpG@PNV group all succumbed to death by day 29 (Figure 5D).

DC stimulation and T cell activation could increase the amount of related proinflammatory cytokines such as IL-12p70

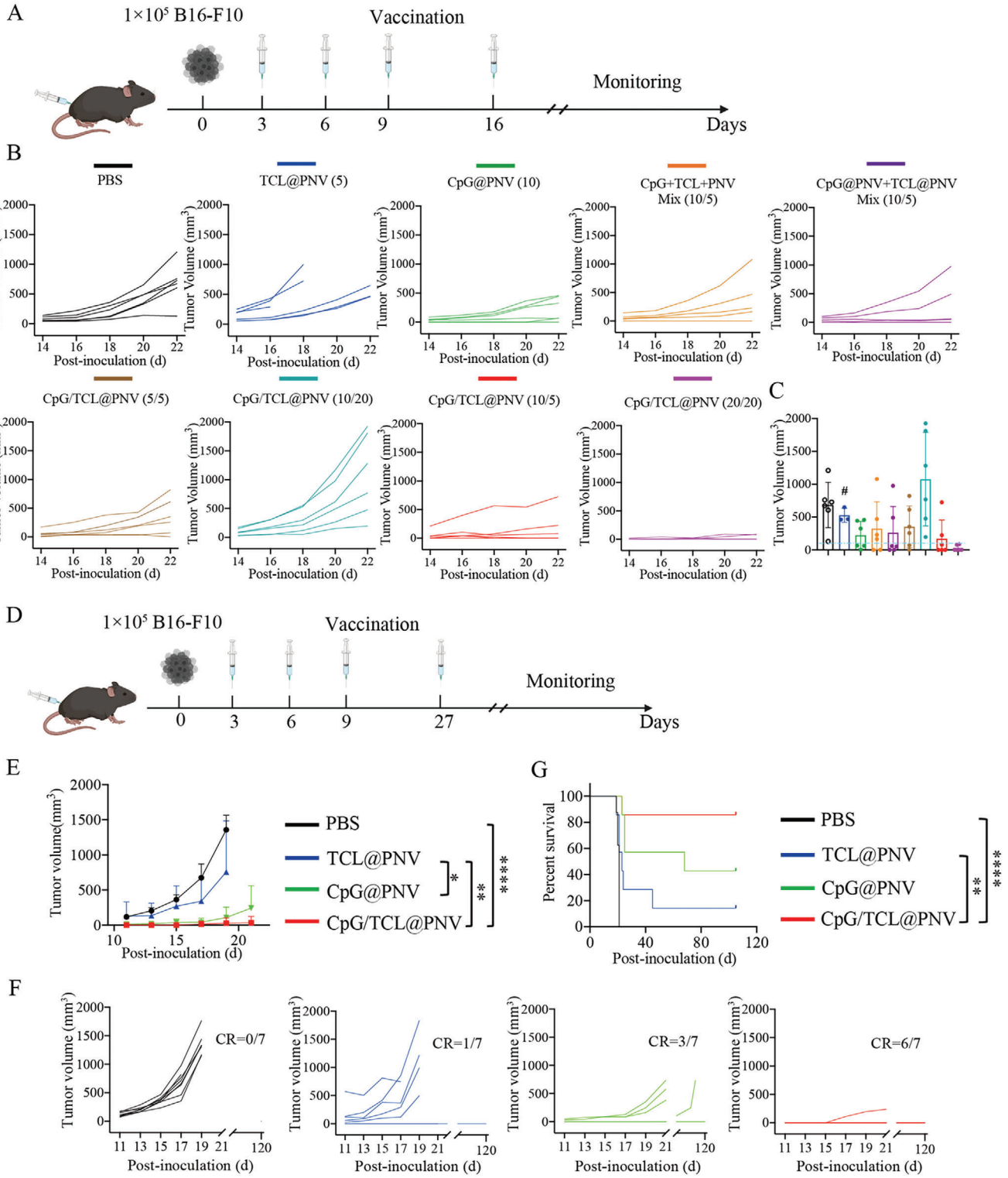

Figure 3. PNVs significantly improve therapeutic efficacy for solid tumors. C57BL/6 mice ($n = 6$) were inoculated with 1×10^5 B16-F10 cells subcutaneously and treated at tail base on days 3, 6, 9, and 16 with PNVs only loaded with antigen (TCL@PNV), PNV only loaded with adjuvant (CpG@PNV), physical mixture of empty PNV with free CpG and TCL (CpG + TCL + PNV Mixture), mixture of CpG@PNV and TCL@PNV (CpG@PNV + TCL@PNV), or PNVs coloading CpG and TCL (CpG/TCL@PNV). A) Timeline for nanovaccine treatment in murine melanoma model. B) Tumor growth curve and C) tumor volume at day 22 after inoculation. # indicates three mice died before day 22. D–G) C57BL/6 mice ($n = 7$) were inoculated with 1×10^5 B16-F10 cells subcutaneously at the right flank and treated on days 3, 6, 9, and 27 with PBS, TCL@PNV, CpG@PNV, or CpG/TCL@PNV. (D) Timeline for treatment experiment. (E, F) Tumor growth curve and (G) survival curve.

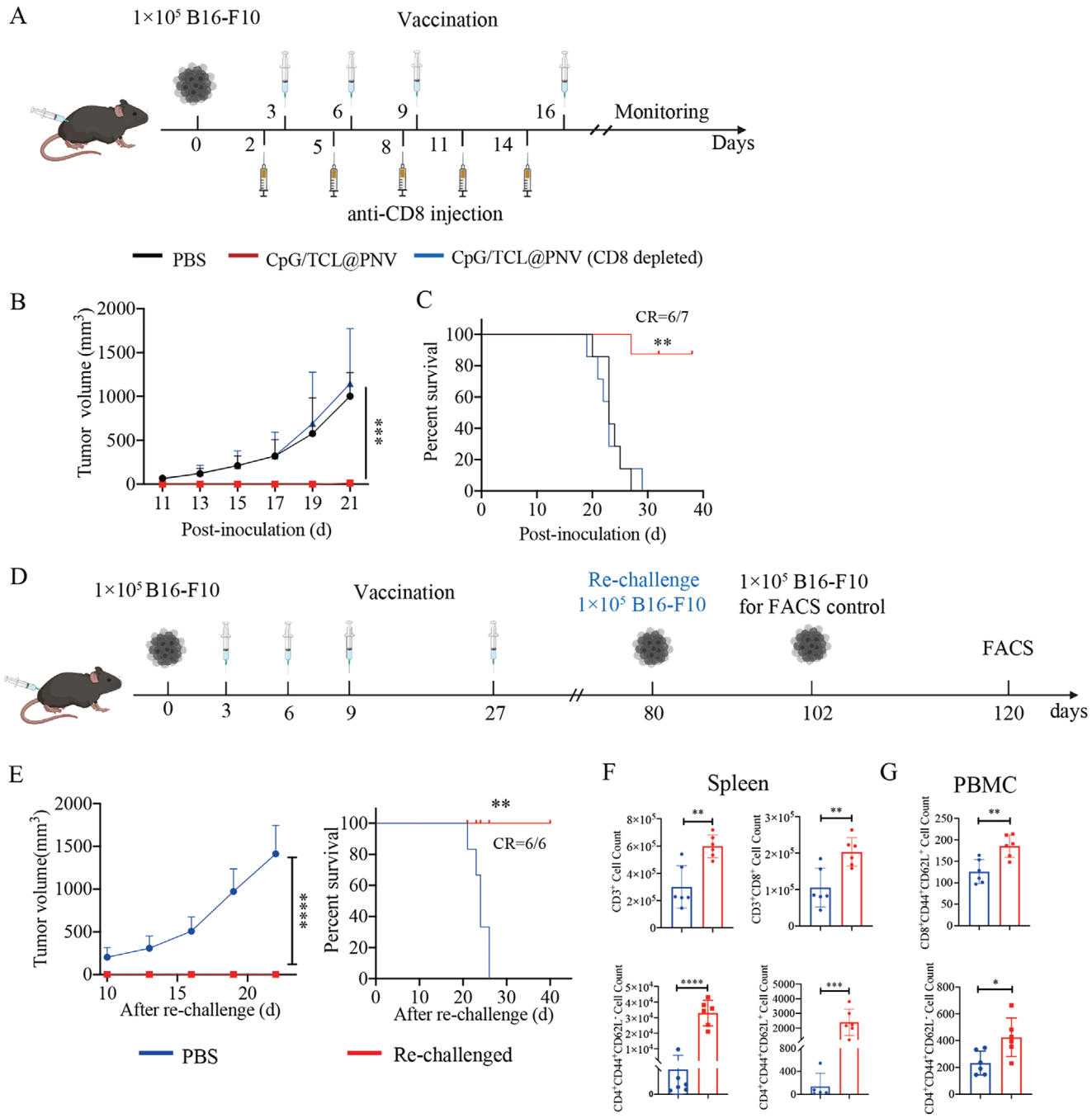

Figure 4. PNVs generate CD8$^+$ T-cell-dependent antitumor efficacy and long-term immune memory. A–C) C57BL/6 mice ($n = 7$) were inoculated with 1×10^5 B16-F10 cells subcutaneously and treated on days 3, 6, 9, and 16 with CpG/TCL@PNV. CD8 antibody was intraperitoneally injected (100 μg per mouse) every three days from day 2 for total 5 times. (A) Experiment timeline, (B) tumor growth curve, and (C) survival curve for nanovaccine therapy with CD8$^+$ T cell depletion. Statistical analysis was compared to PBS group. D–G) Six tumor-bearing mice cured by CpG/TCL@PNV were rechallenged with 1×10^5 B16-F10 cells subcutaneously at the left flank on day 80. (D) Timeline for rechallenge experiment. (E) Tumor growth curve and survival curve for the rechallenge stage. Analysis of memory T cells in (F) spleens or (G) PBMC of survived mice.

and IL-6 in serum. Concentration of serum IL-12p70 and IL-6 from codelivery group CpG/TCL@PNV was 2.3-fold and 2.5-fold higher than those from CpG@PNV group, and 17-fold and 3.7-fold higher than TCL@PNV group (Figure 5E). Splenocytes harvested 24 days postinoculation were cocultured with B16-F10 cell lysate to evaluate the number of Ag-specific T cells generated by nanovaccines in spleens. CpG/TCL@PNV increased the number of IFN-γ producing cell by an average of twofold compared with the single component vaccines based on ELISpot assay (Figure 5F). These results demonstrated

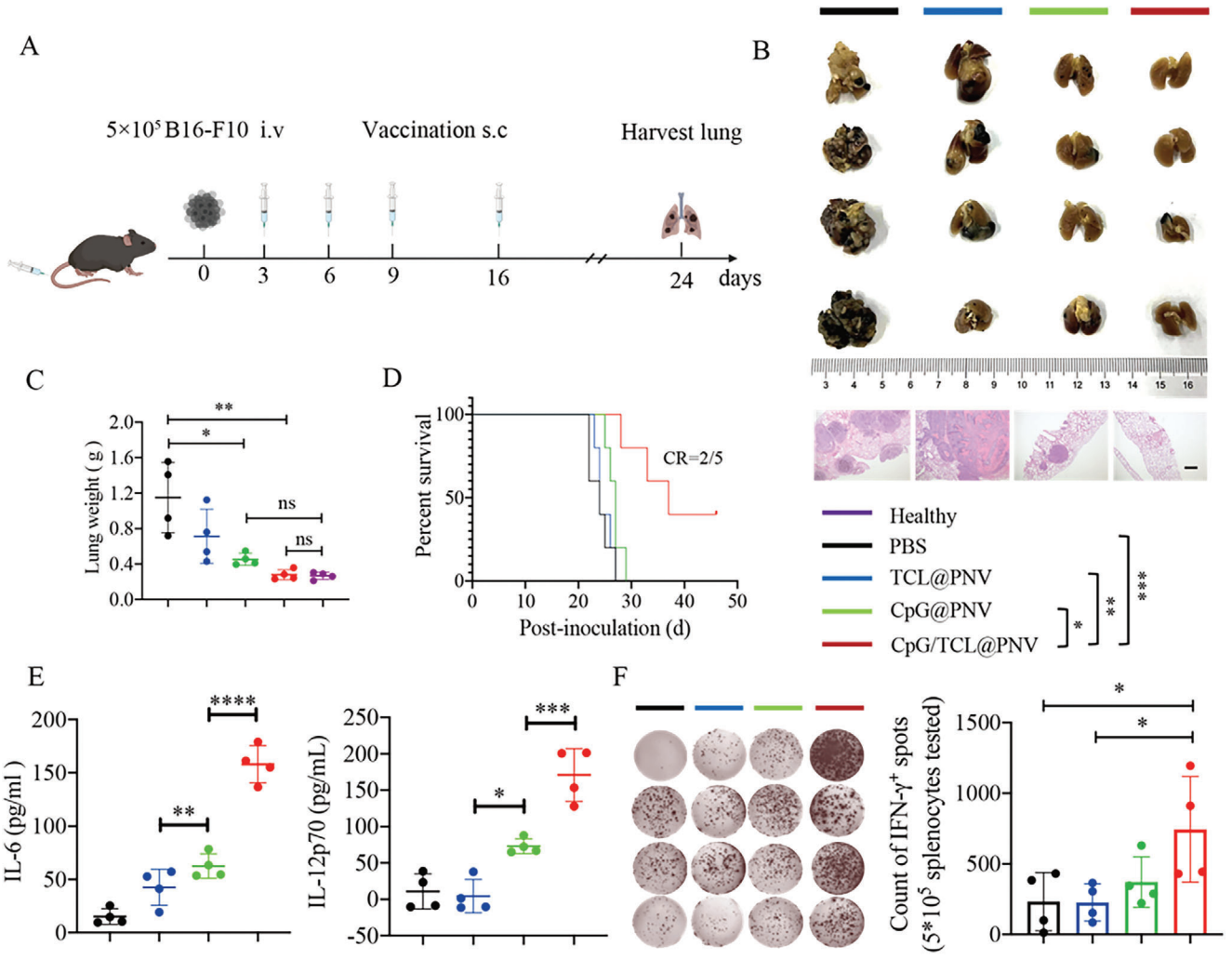

Figure 5. PNVs suppress tumor metastasis. C57BL/6 mice ($n = 9$) were inoculated with 5×10^5 B16-F10 cells intravenously and subaxillary injected with PBS, TCL@PNV, CpG@PNV, or CpG/TCL@PNV on days 3, 6, 9, and 16. A) Timeline of nanovaccine therapy in lung metastasis model. B) Image of harvested lungs and H&E staining of lung histological sections for respective group. Scale bar, 500 μm. C) Lung weight ($n = 4$) in the end of the experiment and D) survival curve ($n = 5$). E) Serum concentration of proinflammatory cytokine IL-6 and IL-12p70 on day 24 ($n = 4$). F) Ag-specific T cell response measured by IFN-γ^+ ELISpot assay and quantification of the spots ($n = 4$).

that PNVs codelivering Ag and CpG were effective in treating metastasis.

2.7. PNVs Loading OVA/CpG Inhibit Growth of OVA-Expressing Tumor

In addition to undefined Ag TCL, PNV platform is also applicable to deliver Ags with known identities. OVA, a model protein was employed as Ag in PNVs to treat subcutaneous B16-OVA tumor (**Figure 6A**). CpG/OVA@PNV (20/5) elicited CR in 71% of tumor-bearing mice, while only 29% of mice were cured by CpG@PNV and OVA@PNV did not cure any mice (Figure 6B,C). Thus, codelivery of OVA and CpG by PNVs substantially improved therapeutic efficacy to OVA-expressing tumor, demonstrating the feasibility of using PNVs to deliver defined Ags.

In addition, CpG/OVA@PNV could also serve as prophylactic cancer vaccine. C57BL/6 mice were immunized with CpG/OVA@PNV and then randomly divided into groups before inoculation with B16-OVA or B16-F10 cells, respectively (Figure 6D). As the Ag used in immunization was OVA, OVA-specific antitumor immune response was generated by PNVs. Therefore, among the two types of tumors, CpG/OVA@PNV inhibited the growth of B16-OVA tumor more effectively (Figure 6E). CpG/OVA@PNV prevented tumor outgrowth in 57% of mice in B16-OVA group, while only 14% of mice were tumor-free in B16-F10 group (Figure 6E,F). The antitumor efficacy observed in mice bearing B16-F10 tumor was probably due to CpG-boosted immune responses against endogenous Ags. All these data demonstrated that PNVs could also load known Ags to serve as both therapeutic and prophylactic vaccines for treating tumors expressing identified Ags.

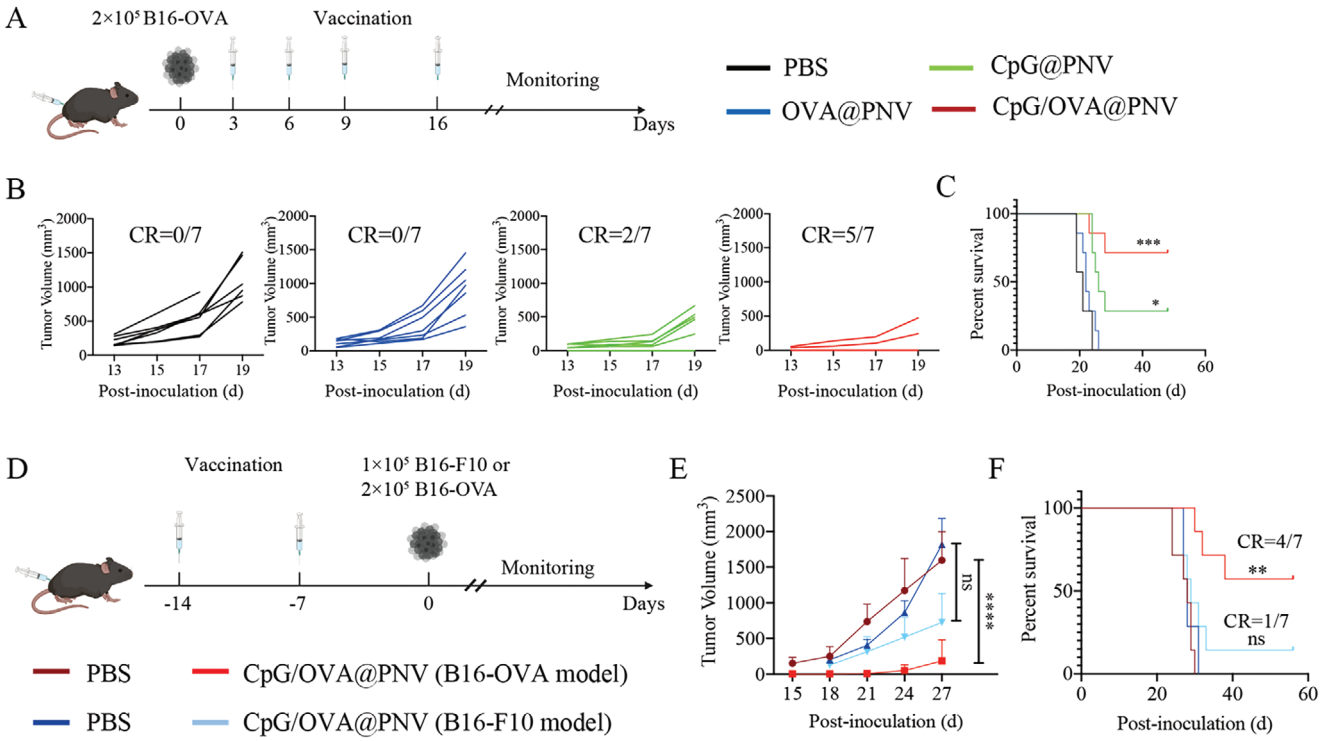

Figure 6. PNVs loading OVA display excellent therapeutic and prophylactic efficacy to OVA-expressing tumor. A–C) C57BL/6 mice ($n = 7$) were inoculated with 2×10^5 B16-OVA cells subcutaneously and treated with PBS, OVA@PNV, CpG@PNV, or CpG/OVA@PNV on days 3, 6, 9, and 16. (A) Timeline, (B) tumor growth curve, and (C) survival curve for PNV treatment in B16-OVA melanoma model. Statistical analysis was compared with PBS. D–F) C57BL/6 mice ($n = 7$) were immunized with CpG/OVA@PNV on days −14 and −7. Immunized mice were randomly divided into groups for tumor inoculation (1×10^5 B16-F10 cells or 2×10^5 B16-OVA cells). (D) Experiment timeline, (E) tumor growth curve, and (F) survival curve for evaluating efficacy of PNVs as prophylactic vaccine. Statistical analysis of CpG/OVA@PNV (B16-OVA model) and CpG/OVA@PNV (B16-F10 model) were compared with PBS groups in red line and blue line, respectively.

3. Discussion

TCLs are ideal for developing personalized cancer vaccines due to their complete coverage of TSAs and ease to be used without prior knowledge of Ag identity.[3a,4d] However, TCL-based vaccines yielded disappointing results in early clinical trials due to the difficulties in quantitative coloading and codelivering TCL/adjuvant to LN DCs.[5,6] Focus was then shifted to indirect approaches utilizing TCL-pulsed DCs according to the number of registered trials. Unfortunately, TCL-loaded DC vaccines still elicit generally poor antigen presentation and transient antitumor immune responses.[15] The limiting factors such as poor LN-targeted migration and high mortality rate of DCs after injection are still difficult to address with current technologies.[16] Therefore, TCL-based vaccines are regaining interests recently and approaches substantially enhancing quantitative control over codelivering of TCL/adjuvant to LN DCs might rekindle the hope of curing cancer patients by TCL-based vaccines.

PNVs were able to elicit strong DC activation and robust antitumor immunity due to four key features. First, PNVs could coload TCL and adjuvant CpG with strikingly high efficiency. Self-assembled PNVs had spermine located in the core to interact with TCL components and charged CpG via electrostatic interactions and hydrogen bonding. When prepared polymer was mixed with TCL and CpG at 5 wt% (10 wt% in total), 98% TCL and 100% CpG were loaded into PNVs together. Similarly, the DLE for model Ag OVA in the presence of CpG was also near 100%, indicating that PNVs are versatile in loading various combinations of Ag and adjuvant. Second, by coencapsulating TCL and adjuvant in the core, PNV protected cargos from enzymatic degradation better than adhering TCL on the surface of carriers.[4b,8,11c,12b]

The near 100% coloading efficiency and preservation of cargo integrity allowed PNVs to quantitatively coload and codeliver TCL/adjuvant by just adjusting the amount of respective cargo added. Codelivery and more importantly the ratio of codelivered Ag and adjuvant are crucial to the antitumor efficacy of vaccines.[6b,8,17] It has been reported that incorrect ratio of Ags and adjuvant might promote immune tolerance or autoimmune diseases.[6a,9,10,18] We also observed that despite CpG/TCL@PNV (10/20) had fourfold higher TCL loading than CpG/TCL@PNV (10/5), CpG/TCL@PNV (10/20) elicited much weaker efficacy (Figure 3B,C). However, CpG/TCL@PNV (20/20), with both CpG and TCL amount increased, outperformed CpG/TCL@PNV (10/5). Therefore, PNVs can provide a convenient tool to tailor the ratio of TCL/adjuvant delivered to the same DC, thus significantly enhancing therapeutic efficacies and shedding insight into rational design of future vaccines. Furthermore, high coloading efficiency and well protection of cargo endowed PNVs to make full use of available stringent amount of TCL when tumor biopsy is

difficult to harvest from early, diffused, deep internal, or difficult-to-resect tumors.

Third, PNVs demonstrated excellent targeting ability to LNs and induced 50% of loaded CpG to accumulate in iLNs, exhibiting 20-fold higher LN-directed delivery than free CpG. The LN-targeting efficiency of PNVs was significantly higher than most published nanovaccines and could even match to the most efficient LN-targeting carriers in literature.[13] The superior LN targetability of PNVs is likely a result of favorable size (about 55 nm)[13d] and hydrophilic surface with moderate negative surface charge (−6.6 mV).[13d,19,20]

Fourth, the DTC component in designed polymer PEG–p(TMC-DTC)–Spermine allowed cross-linking of nearby polymers in PNVs via disulfide bond, thus stabilizing the structure of PNVs in circulation. Once PNVs are uptaken by DCs, the disulfide bonds dissociate in response to the reducing cytosol environment and rapidly release TCL and CpG to enhance DC priming.[21]

All these properties allowed PNVs to generate potent antitumor efficacies. CpG/TCL@PNVs cured 85% mice in subcutaneous melanoma model, elicited 40% CR in lung metastasis model, and protected 100% cured mice from tumor recurrence. Notably, PNVs elicited such efficacy even in the absence of immune checkpoint inhibitors and at a relative low dose compared to other TCL-based vaccines.[4b,11a,d,22] In addition, PNVs did not elicit overt toxicities both in vitro and in vivo (Figures S2 and S3, Supporting Information) and are safe to be used.

4. Conclusion

In summary, we developed PNVs to quantitatively coload and ratio-controlled codeliver TCL/adjuvant to LNs, thus inducing robust and specific antitumor immune responses. Not only did CpG/TCL@PNV substantially improve therapeutic outcomes in both solid tumor and metastasis models, PNVs also generated long-term antitumor immune memory to prevent tumor recurrence. PNV platform is also applicable to load defined Ag and adjuvant to serve as both therapeutic and preventive vaccines. The potent and versatile PNVs have high potential for clinical translation and might provide new opportunities for curing cancer patients.

5. Experimental Section

Materials: CpG (5′-TCCATGACGTTCCTGACGTT-3′) and dye-labeled CpG containing a full phosphorothioate backbone were synthesized from Sangon Biotech. Lysis buffer NP-40 (Nonidet P 40, cat. P0013F) and PMSF (Phenylmethanesulfonyl fluoride, cat. ST506) were purchased from Beyotime. OVA (cat. A7641) was purchased from Sigma-Aldrich. Mouse enzyme-linked immunosorbe assay (ELISA) kit for IL-12p70 (cat. 88-7121-88) and IL-6 (cat. 88-7064-88) were purchased from Thermo Fisher. IFN-γ^+ ELISpot assay kit (cat. 2210005) was purchased from Dakewe. Anti-mouse antibody CD16/32 (clone.93), CD11c–fluorescein isothiocyanate (FITC) (clone. N418), CD80–Allophycocyanin (APC) (clone.16-10A1), CD86–PE/Cy7 (clone. GL-1), SIINFEKL/H-2K^b–Allophycocyanin (PE) (clone. 25-D1.16), CD3–FITC (clone. 17A2), CD4–FITC (clone. GK1.5), CD8α–PE/Cy7 (clone. 53-6.7), CD8α–APC/Cy7 (clone. 53-6.7), CD8α–PE (clone. 53-6.7), CD44–PE (clone. IM7), CD62L–APC/Cy7 (clone. MEL-14), CD25–PE (clone. PC61), IFN-γ^+–APC (clone. XMG 1.2), and isotype control Immunoglobulin G (IgG), κ-PE (clone. MOPC-21) were purchased from Biolegend. Anti-mouse CD8α (cat. BP004-1) was purchased from BioXcell. Recombinant protein murine granulocyte-macrophage colony stimulating factor (GM-CSF) (cat. 250-05) was purchased from Peprotech.

Cell Lines and Animals: B16-F10 cells were purchased from American Type Culture Collection. B16-OVA cells were kindly provided by Tong Shen from the Soochow University. B16-OVA and B16-F10 cells were cultured in roswell park memorial institute (RPMI)-1640 medium containing 10% FBS, 1% penicillin, 1% streptomycin. 293T and L929 cell lines were cultured in dulbecco's modified eagle medium (DMEM) and minimum essential medium (MEM), respectively, containing 10% FBS, 1% penicillin, and 1% streptomycin. Female C57BL/6 (6–8 weeks) were purchased from Charles River company (Beijing, China) and maintained under protocols approved by the Soochow University Laboratory Animal Center. OT-1 mice were purchased from Shanghai Model Organisms Center (Shanghai, P. R. China). All animal experiments were approved by the Animal Care and Use Committee of Soochow University and all protocols conformed to the Guide for the Care and Use of Laboratory Animals.

Synthesis and Characterization of CpG/Antigen@PNVs: PEG–P(TMC-DTC)–SP was synthesized as reported previously.[23] Briefly, preparation of block copolymers was by ring open polymerization of TMC and DTC through the macromolecular initiators. TCL were obtained by lysing B16-F10 cells with NP-40 lysis buffer in PMSF solution (1 mM). After digestion 30 min on ice, cell lysates were centrifuged at 13 000 rpm and supernatant was harvested. The concentration of TCL in supernatant was determined by using micro bicinchoninic Acid (BCA) protein assay kit. To prepare CpG/TCL@PNV with theoretical loading at 5.0 wt%, 100 µL PEG–P(TMC-DTC)–SP (40 mg mL^{-1}) in DMF was added into *N*-2-hydroxylethylpiperazine-*N*-ethane-sulfonic acid buffer (pH 6.8, 5 mM, 900 µL) containing TCL (2 mg mL^{-1}, 200 µg) and CpG (2 mg mL^{-1}, 200 µg) under stirring at 300 rpm. After stirring at room temperature (RT) for 10 min, the dispersion was dialyzed against PBS (pH 7.4, 10 mM) for 6 h (molecular weight cut off, MWCO 1000 kDa) to remove DMF and unencapsulated CpG/TCL. Size distribution was measured by DLS. The amounts of TCL and CpG loaded were determined by micro BCA protein assay kit and nanodrop, respectively. Drug loading content (DLC) and DLE were calculated based on the following formula

$$\text{DLC (wt\%)} = \frac{\text{weight of loaded drug}}{\text{total weight of loaded drug and polymers}} \times 100\ (\%) \quad (1)$$

$$\text{DLE (\%)} = \frac{\text{weight of loaded drug}}{\text{weight of drug in feed}} \times 100\ (\%) \quad (2)$$

Cy5-labeled OVA was employed to prepare the OVA^{Cy5}@PNV. Reduction-triggered OVA release from OVA^{Cy5}@PNV (nanoparticle conc: 1 mg mL^{-1}, $n = 3$) was evaluated via dialysis against 10 mM GSH in phosphate buffer (PB) and incubated at RT with gentle shaking on an orbital shaker. Release of OVA^{Cy5} was measured by a fluorescence spectrometer. The size changes of nanoparticles in 10% FBS or 10 mM GSH were measured by DLS.

Evaluation of Nanovaccine Uptake by BMDCs and Activation of BMDCs: BMDCs were obtained from marrow of C57BL/6 mice. The femurs and tibias of the mice were aseptically dissected and flushed with a syringe to obtain bone marrow (BM) cells. To generate BMDCs, BM cells were cultured in RPMI-1640 medium containing 10% FBS, 1% penicillin, 1% streptomycin, and 20 ng mL^{-1} recombinant mouse GM-CSF. The medium was all replaced after 48 h and then half replaced every 48 h. Nonadherent or loosely attached BMDCs were collected on day 7.

BMDCs were plated in glass-bottomed dish (1 × 10^6 per well) and cultured with CpG^{Cy5}@PNV or mixture of empty PNV and free CpG^{Cy5} (0.15 µM). After being cocultured for 4 or 24 h, cells were further cultured with 0.5 nM lysotracker green at 37 °C with 5% CO_2 for 30 min. BMDCs were then washed with cold PBS and fixed with 4% paraformaldehyde solution for 15 min, then treated with 5 µg mL^{-1} 4′,6-diamidino-2-phenylindole (DAPI) for 10 min (each step was followed by PBS washing ×3) before confocal laser scanning microscope (CLSM) observation. FITC-labeled OVA (OVA^{FITC}) was loaded into PNV to form OVA^{FITC}@PNV. BMDCs (1 × 10^6

per well) were cultured with free OVA^{FITC} or the equivalent dose of OVA in the form of OVA^{FITC}@PNV for 24 h before flow cytometry analysis.

Immature BMDCs were cultured in 24-well plates (2×10^6 per well). After 8 h, BMDCs were incubated with PBS, OVA@PNV, CpG@PNV, CpG/OVA@PNV, as well as physical mixture of empty PNV, CpG, and OVA (weight ratio of PNV:CpG:OVA = 20:1:1, CpG or OVA 0.5 μg mL^{-1}, $n = 3$) at 37 °C with 5% CO_2. After 20 h, cells were centrifuged and washed with fluorescence activated cell sorting (FACS) buffer (1% FBS in PBS), incubated with anti-CD16/32 at RT, and then stained with CD11c–FITC, CD80–APC, CD86–PE/Cy7, and SIINFEKL/H-$2K^b$–PE for 20 min at RT. Cells were then washed twice by FACS buffer and detected by flow cytometer. Culture medium was harvested for IL-12p70 and IL-6 ELISA assay.

Nanovaccines Boost the T Cell Activation Ability of BMDCs In Vitro: BMDCs (1×10^6 cells) were treated with PBS, OVA@PNV (0.5 μg OVA mL^{-1}), CpG@PNV (0.5 μg CpG mL^{-1}), or CpG/OVA@PNV (0.5 μg OVA and 0.5 μg CpG mL^{-1}), respectively, at 37 °C with 5% CO_2 ($n = 3$). After 20 h, $CD8^+$ T cells were isolated from OT-1 splenocytes and cocultured with BMDCs from different groups. After 24 h, cells were harvested from each well, washed, and added with counting beads before staining with CD3–FITC, CD8–PE, and IFN-γ^+–APC. The number of IFN-γ^+ T cells was accessed via flow cytometer.

Biosafety of CpG/OVA@PNV In Vitro: 293T cells or L929 cells were incubated overnight in 96-well plates with 3000 cells per well. PNVs were added in different concentrations (5, 10, 50, 100 μg mL^{-1}) for coculturing for another 24 h. Cell viability was analyzed via cell counting kit (CCK)-8 cytotoxicity assay following manufacturer's instruction ($n = 6$). Optical density (OD) of samples were measured.

$$\text{Cell viability } (\%) = \frac{\text{OD experiment} - \text{OD blank}}{\text{OD control} - \text{OD blank}} \times 100\ (\%) \quad (3)$$

LN-Targeting and In Vivo DC Activation Ability of PNVs: C57BL/6 mice ($n = 4$–5) were injected with PBS, free CpG^{Cy7}, and PNVs loading CpG^{Cy7} (20 μg CpG per mouse) in tail base and euthanatized 24 h postinjection. Inguinal LNs and other organs were harvested for in vivo imaging system (IVIS) imaging.

Mice ($n = 3$) were administrated with PBS, mixture of free CpG, OVA, and empty PNV (CpG + OVA + PNV Mixture), OVA@PNV, and CpG/OVA@PNV in tail base (20 μg CpG and 5 μg OVA per mouse). Mice were euthanatized after 24 h and inguinal LNs were ground into single-cell suspensions in ice PBS. Cells were then stained with fluorescently labeled antibodies mentioned in the previous session and analyzed via flow cytometry.

Evaluation of PNV-Induced Antigen-Specific T Cells in Spleen: Two sets of experiments were conducted. C57BL/6 mice inoculated with 2×10^5 B16-OVA and B16-F10 cells were immunized with CpG/OVA@PNV and CpG/TCL@PNV, respectively, on days 3, 6, and 9. TCL was generated from B16-F10 cells. Spleens from both sets of experiments were harvested on day 16.

The number of Ag-specific T cells (IFN-γ^+) in spleen was determined by ELISpot assay. According to the manufacturer's instructions, splenocytes were seeded in 96-well plates (10^5 cells per well) precoated with mouse anti-IFN-γ antibody. Splenocytes were stimulated with 25 μg mL^{-1} OVA or TCL for 24 h. A biotinylated antibody specific for IFN-γ and alkaline phosphatase conjugated to streptavidin were subsequently used to detect the secreted IFN-γ.

Splenocytes were also plated in 24-well plates (2×10^6 per well) and pulsed with OVA or TCL. After 72 h, cells were centrifuged and washed with FACS buffer, incubated with anti-CD16/32 at RT, and then stained with CD3–FITC, CD8–APC/Cy7, and CD25–PE. Cells were then washed twice by FACS buffer and analyzed by a flow cytometer.

Evaluation of Antitumor Efficacy of PNVs: For therapeutic studies, TCL was lysed from B16-F10 cells as described above. CpG and TCL were co-encapsulated at different ratios. CpG/TCL@PNV (10/5) meant administration of PNVs loading 10 μg CpG and 5 μg TCL per mouse. The prepared ratios included 5/5, 10/5, 10/20, and 20/20.

For B16-F10 model, C57BL/6 mice were inoculated subcutaneously with 1×10^5 B16-F10 cells on the right flank per mouse at day 0 and then immunized with nanovaccines on days 3, 6, 9, and 16. Tumor growth was monitored every other day and tumor volume was calculated by the following equation: tumor volume = length × $\text{width}^2 \times 0.5$. For $CD8^+$ T cell depletion study, C57BL/6 mice were inoculated subcutaneously with 1×10^5 B16-F10 cells on the right flank at day 0 and then immunized with different vaccine formulations on days 3, 6, 9, and 16. CD8 antibody was intraperitoneally injected with 100 μg per mouse every three days from day 2 for 5 times.

For B16-OVA tumor model, C57BL/6 mice were inoculated subcutaneously with 2×10^5 B16-OVA cells on the right flank of mice at day 0 and then immunized with nanovaccines on days 3, 6, 9, and 16.

For tumor metastasis model, C57BL/6 mice were inoculated intravenously with 5×10^5 B16-F10 cells on day 0 and then immunized with PNVs on days 3, 6, 9, and 16. Four mice were randomly chosen from each group and euthanatized. Lungs were harvested and fixed with 4% paraformaldehyde solution on day 24 postinoculation. Lungs were weighted after fixation for 7 days. H&E staining was prepared by Servicebio. Cytokine IL-12p70 and IL-6 in serum were determined by ELISA kit. Splenocytes were collected on day 24 postinoculation and seeded in a 96-well plate (5×10^5 cells per well). After coculturing with TCL for 24 h, IFN-γ secreted by splenocytes was determined by ELISpot assay as previously introduced.

Evaluation of PNV-Induced Long-Term Immune Memory: C57BL/6 mice were subcutaneously inoculated with 1×10^5 B16-F10 cells on the right flank on day 0 and immunized with nanovaccines on days 3, 6, 9, and 27. Six cured mice were rechallenged by inoculation of 1×10^5 B16-F10 cells on the left flank at day 80 post initial tumor inoculation. PBMCs and splenocytes were collected at day 120 and resuspended in ammonium-chloride-potassium (ACK) lysis buffer to remove red blood cells. Cells were then centrifuged and resuspended with counting beads (10 000 per well) in FACS buffer. After being centrifuged at 1200 *g* for 4 min, cells were incubated with anti-CD16/32 at RT and stained with CD4–FITC, CD8–PE/Cy7, CD44–PE, and CD62L–APC/Cy7. Cells were then washed twice by FACS buffer and analyzed by flow cytometer.

Protective Effects of PNVs: For prophylactic study, C57BL/6 mice were immunized by CpG/OVA@PNV vaccine twice on days −14 and −7. Mice were then randomly divided into groups and were subcutaneously inoculated with 2×10^5 B16-OVA cells or 1×10^5 B16-F10 cells, respectively, on the right flank at day 0. Tumor growth was monitored every other day.

Statistical Analysis: All data were presented as mean ± standard deviation. Unless otherwise indicated, significant differences among groups were evaluated by one-way analysis of variance (ANOVA) with Tukey multiple comparison tests, and the survival rate was analyzed by Kaplan–Meier technique with a log-rank test for comparison using GraphPad Prism (version 8). *, $p < 0.05$; **$p < 0.01$; ***$p < 0.001$, and ****$p < 0.0001$.

Supporting Information

Supporting Information is available from the Wiley Online Library or from the author.

Acknowledgements

This work was financially supported by the National Key R&D Program of China (Grant No. 2021YFB3800900), the National Natural Science Foundation of China (Grant Nos. 52233007, 82150410455), and Priority Academic Program Development (PAPD) of Jiangsu Higher Education Institutions.

Conflict of Interest

The authors declare no conflict of interest.

Author Contributions

G.C., Y.Z., and Z.Z. conceived and designed the experiments. G.C., Y.P.S., L.Q., C.S., and Y.S. performed the experiments. G.C., Y.Z., and Z.Z. ana-

lyzed and processed the data. F.M. provided advice in designing and conducting experiments. G.C., Y.Z., and Z.Z. wrote and revised the paper.

Data Availability Statement

The data that support the findings of this study are available from the corresponding author upon reasonable request.

Keywords

cancer vaccines, immunotherapy, lymph node targeting, polymersomes, targeted delivery

Received: October 25, 2023
Revised: February 29, 2024
Published online: May 2, 2024

[1] a) L. A. Rojas, Z. Sethna, K. C. Soares, C. Olcese, N. Pang, E. Patterson, J. Lihm, N. Ceglia, P. Guasp, A. Chu, R. Yu, A. K. Chandra, T. Waters, J. Ruan, M. Amisaki, A. Zebboudj, Z. Odgerel, G. Payne, E. Derhovanessian, F. Mueller, I. Rhee, M. Yadav, A. Dobrin, M. Sadelain, M. Luksza, N. Cohen, L. Tang, O. Basturk, M. Goenen, S. Katz, et al., *Nature* **2023**, *618*, 144; b) U. Sahin, P. Oehm, E. Derhovanessian, R. A. Jabulowsky, M. Vormehr, M. Gold, D. Maurus, D. Schwarck-Kokarakis, A. N. Kuhn, T. Omokoko, L. M. Kranz, M. Diken, S. Kreiter, H. Haas, S. Attig, R. Rae, K. Cuk, A. Kemmer-Brueck, A. Breitkreuz, C. Tolliver, J. Caspar, J. Quinkhardt, L. Hebich, M. Stein, A. Hohberger, I. Vogler, I. Liebig, S. Renken, J. Sikorski, M. Leierer, et al., *Nature* **2020**, *585*, 107; c) A. Khattak, M. Carlino, T. Meniawy, G. Ansstas, T. Medina, M. H. Taylor, K. B. Kim, M. McKean, G. V. Long, R. J. Sullivan, M. Faries, T. Tran, C. Cowey, A. Pecora, J. Segar, V. Atkinson, G. T. Gibney, J. Luke, S. Thomas, E. Buchbinder, P. Hou, L. Zhu, T. Zaks, M. Brown, P. Aanur, R. S. Meehan, J. S. Weber, *Cancer Res.* **2023**, *83*, CT001.

[2] a) M. J. Lin, J. Svensson-Arvelund, G. S. Lubitz, A. Marabelle, I. Melero, B. D. Brown, J. D. Brody, *Nat. Cancer* **2022**, *3*, 911; b) M. Saxena, S. H. van der Burg, C. J. M. Melief, N. Bhardwaj, *Nat. Rev. Cancer* **2021**, *21*, 360.

[3] a) E. Blass, P. A. Ott, *Nat. Rev. Clin. Oncol.* **2021**, *18*, 215; b) D. Karan, *Vaccine* **2017**, *35*, 5794; c) M. Peng, Y. Mo, Y. Wang, P. Wu, Y. Zhang, F. Xiong, C. Guo, X. Wu, Y. Li, X. Li, G. Li, W. Xiong, Z. Zeng, *Mol. Cancer* **2019**, *18*, 674.

[4] a) L. Diao, M. Liu, *Adv. Sci.* **2023**, *10*, 2300121; b) L. Ma, L. Diao, Z. Peng, Y. Jia, H. Xie, B. Li, J. Ma, M. Zhang, L. Cheng, D. Ding, X. Zhang, H. Chen, F. Mo, H. Jiang, G. Xu, F. Meng, Z. Zhong, M. Liu, *Adv. Mater.* **2021**, *33*, 2104849; c) I. Salewski, Y. S. Gladbach, S. Kuntoff, N. Irmscher, O. Hahn, C. Junghanss, C. Maletzki, *J. Transl. Med.* **2020**, *18*, 402; d) Y. Zheng, Z. Zhong, *J. Controlled Release* **2022**, *347*, 308.

[5] V. K. Sondak, J. A. Sosman, *Semin. Cancer Biol.* **2003**, *13*, 409.

[6] a) C. B. Chesson, A. Zloza, *Nanomedicine* **2017**, *12*, 2693; b) M. E. Aikins, C. Xu, J. J. Moon, *Acc. Chem. Res.* **2020**, *53*, 2094.

[7] a) H. Liu, K. D. Moynihan, Y. Zheng, G. L. Szeto, A. V. Li, B. Huang, D. S. Van Egeren, C. Park, D. J. Irvine, *Nature* **2014**, *507*, 519; b) N. Gong, Y. Zhang, X. Teng, Y. Wang, S. Huo, G. Qing, Q. Ni, X. Li, J. Wang, X. Ye, T. Zhang, S. Chen, Y. Wang, J. Yu, P. C. Wang, Y. Gan, J. Zhang, M. J. Mitchell, J. Li, X.-J. Liang, *Nat. Nanotechnol.* **2020**, *15*, 1053; c) S. L. Liu, Q. Jiang, X. Zhao, R. F. Zhao, Y. N. Wang, Y. M. Wang, J. B. Liu, Y. X. Shang, S. Zhao, T. T. Wu, Y. L. Zhang, G. J. Nie, B. Q. Ding, *Nat. Mater.* **2021**, *20*, 431; d) R. Kuai, L. J. Ochyl, K. S. Bahjat, A. Schwendeman, J. J. Moon, *Nat. Mater.* **2017**, *16*, 489; e) G. M. Lynn, C. Sedlik, F. Baharom, Y. Zhu, R. A. Ramirez-Valdez, V. L. Coble, K. Tobin, S. R. Nichols, Y. Itzkowitz, N. Zaidi, J. M. Gammon, N. J. Blobel, J. Denizeau, P. de la Rochere, B. J. Francica, B. Decker, M. Maciejewski, J. Cheung, H. Yamane, M. G. Smelkinson, J. R. Francica, R. Laga, J. D. Bernstock, L. W. Seymour, C. G. Drake, C. M. Jewell, O. Lantz, E. Piaggio, A. S. Ishizuka, R. A. Seder, *Nat. Biotechnol.* **2020**, *38*, 320.

[8] C. E. Callmann, L. E. Cole, C. D. Kusmierz, Z. Huang, D. Horiuchi, C. A. Mirkin, *Proc. Natl. Acad. Sci. USA* **2020**, *117*, 17543.

[9] N. K. Mehta, R. V. Pradhan, A. P. Soleimany, K. D. Moynihan, A. M. Rothschilds, N. Momin, K. Rakhra, J. Mata-Fink, S. N. Bhatia, K. D. Wittrup, D. J. Irvine, *Nat. Biomed. Eng.* **2020**, *4*, 636.

[10] a) J. W. C. Tervaert, M. Martinez-Lavin, L. J. Jara, G. Halpert, A. Watad, H. Amital, Y. Shoenfeld, *Autoimmun. Rev.* **2023**, *22*, 103287; b) S. J. Win, D. G. G. McMillan, F. Errington-Mais, V. K. Ward, S. L. Young, M. A. Baird, A. A. Melcher, *Br. J. Cancer* **2012**, *106*, 92.

[11] a) Y. Ding, J. Yang, H. Wei, J. Wang, S. Huang, S. Yang, Y. Guo, B. Li, X. Shuai, *Small* **2023**, *19*, 2301420; b) X. Hu, T. Wu, X. Qin, Y. Qi, Q. Qiao, C. Yang, Z. Zhang, *Adv. Healthcare Mater.* **2019**, *8*, 1800837; c) X. Wang, N. Wang, Y. Yang, X. Wang, J. Liang, X. Tian, H. Zhang, X. Leng, *Biomater. Sci.* **2019**, *7*, 3062; d) Q. Fan, Q. Ma, J. Bai, J. Xu, Z. Fei, Z. Dong, A. Maruyama, K. W. Leong, Z. Liu, C. Wang, *Sci. Adv.* **2020**, *6*, eabb4639.

[12] a) M. Liu, D. Xie, D. Hu, R. Zhang, Y. Wang, L. Tang, B. Zhou, B. Zhao, L. Yang, *Adv. Sci.* **2023**, *10*, 2207697; b) C. Wu, W. He, Y. Chen, J. Cai, F. Zeng, Z. Lu, J. Wang, *Adv. Healthcare Mater.* **2023**, *12*, 2203026.

[13] a) X. Han, M.-G. Alameh, K. Butowska, J. J. Knox, K. Lundgreen, M. Ghattas, N. Gong, L. Xue, Y. Xu, M. Lavertu, P. Bates, J. Xu, G. Nie, Y. Zhong, D. Weissman, M. J. Mitchell, *Nat. Nanotechnol.* **2023**, *18*, 1105; b) V. Dasari, L. K. McNeil, K. Beckett, M. Solomon, G. Ambalathingal, T. L. Thuy, A. Panikkar, C. Smith, M. P. Steinbuck, A. Jakubowski, L. M. Seenappa, E. Palmer, J. Zhang, C. M. Haqq, P. C. DeMuth, R. Khanna, *Nat. Commun.* **2023**, *14*, 4371; c) Q. Ni, F. Zhang, Y. Liu, Z. Wang, G. Yu, B. Liang, G. Niu, T. Su, G. Zhu, G. Lu, L. Zhang, X. Chen, *Sci. Adv.* **2020**, *6*, eaaw6071; d) A. He, X. Li, Z. Dai, Q. Li, Y. Zhang, M. Ding, Z.-f. Wen, Y. Mou, H. Dong, *J. Nanobiotechnol.* **2023**, *21*, 236.

[14] Y. Yue, J. Xu, Y. Li, K. Cheng, Q. Feng, X. Ma, N. Ma, T. Zhang, X. Wang, X. Zhao, G. Nie, *Nat. Biomed. Eng.* **2022**, *6*, 898.

[15] a) Z. Guo, Y. Yuan, C. Chen, J. Lin, Q. Ma, G. Liu, Y. Gao, Y. Huang, L. Chen, L.-Z. Chen, Y.-F. Huang, H. Wang, B. Li, Y. Chen, X. Zhang, *npj Precis. Oncol.* **2022**, *6*, 34; b) Z. Ding, Q. Li, R. Zhang, L. Xie, Y. Shu, S. Gao, P. Wang, X. Su, Y. Qin, Y. Wang, J. Fang, Z. Zhu, X. Xia, G. Wei, H. Wang, H. Qian, X. Guo, Z. Gao, Y. Wang, Y. Wei, Q. Xu, H. Xu, L. Yang, *Signal Transduction Targeted Ther.* **2021**, *6*, 26; c) J. L. Tanyi, S. Bobisse, E. Ophir, S. Tuyaerts, A. Roberti, R. Genolet, P. Baumgartner, B. J. Stevenson, C. Iseli, D. Dangaj, B. Czerniecki, A. Semilietof, J. Racle, A. Michel, I. Xenarios, C. Chiang, D. S. Monos, D. A. Torigian, H. L. Nisenbaum, O. Michielin, C. H. June, B. L. Levine, D. J. Powel Jr., D. Gfeller, R. Mick, U. Dafni, V. Zoete, A. Harari, G. Coukos, L. E. Kandalaft, *Sci. Transl. Med.* **2018**, *10*, eaao5931.

[16] a) L. Lei, D. Huang, H. Gao, B. He, J. Cao, N. A. Peppas, *Sci. Adv.* **2022**, *8*, eadc8738; b) P. Yang, H. Song, Y. Qin, P. Huang, C. Zhang, D. Kong, W. Wang, *Nano Lett.* **2018**, *18*, 4377.

[17] N. O. Fischer, A. Rasley, M. Corzett, M. H. Hwang, P. D. Hoeprich, C. D. Blanchette, *J. Am. Chem. Soc.* **2013**, *135*, 2044.

[18] D. T. Johnson, J. Zhou, A. V. Kroll, R. H. Fang, M. Yan, C. Xiao, X. Chen, J. Kline, L. Zhang, D.-E. Zhang, *Leukemia* **2022**, *36*, 994.

[19] X. Peng, J. Wang, F. Zhou, Q. Liu, Z. Zhang, *Cell. Mol. Life Sci.* **2021**, *78*, 5139.

[20] T. Nakamura, M. Kawai, Y. Sato, M. Maeki, M. Tokeshi, H. Harashima, *Mol. Pharmaceutics* **2020**, *17*, 944.

[21] a) S. Yue, J. An, Y. Zhang, J. Li, C. Zhao, J. Liu, L. Liang, H. Sun, Y. Xu, Z. Zhong, *Adv. Mater.* **2023**, *35*, 2209984; b) J. Liu, L. Zhang, D. Zhao, S. Yue, H. Sun, C. Ni, Z. Zhong, *J. Controlled Release* **2022**, *350*, 122.

[22] a) Y. Ye, C. Wang, X. Zhang, Q. Hu, Y. Zhang, Q. Liu, D. Wen, J. Milligan, A. Bellotti, L. Huang, G. Dotti, Z. Gu, *Sci. Immunol.* **2017**, *2*, eaan5692; b) M. A. Gleisner, C. Pereda, A. Tittarelli, M. Navarrete, C. Fuentes, I. Ávalos, F. Tempio, J. P. Araya, M. I. Becker, F. E. Gonzalez, M. N. Lopez, F. Salazar-Onfray, *J. Immunother. Cancer* **2020**, *8*, e000999.

[23] H. Qin, Y. Jiang, J. Zhang, C. Deng, Z. Zhong, *Mol. Pharmaceutics* **2019**, *16*, 3711.